

Journal of Materials Chemistry A

Accepted Manuscript



This is an *Accepted Manuscript*, which has been through the Royal Society of Chemistry peer review process and has been accepted for publication.

Accepted Manuscripts are published online shortly after acceptance, before technical editing, formatting and proof reading. Using this free service, authors can make their results available to the community, in citable form, before we publish the edited article. We will replace this *Accepted Manuscript* with the edited and formatted *Advance Article* as soon as it is available.

You can find more information about *Accepted Manuscripts* in the [Information for Authors](#).

Please note that technical editing may introduce minor changes to the text and/or graphics, which may alter content. The journal's standard [Terms & Conditions](#) and the [Ethical guidelines](#) still apply. In no event shall the Royal Society of Chemistry be held responsible for any errors or omissions in this *Accepted Manuscript* or any consequences arising from the use of any information it contains.

ARTICLE

Novel design of silicon-based lithium-ion battery anode for highly stable cycling at elevated temperature

Cite this: DOI: 10.1039/x0xx00000x

Received 00th January 2014,
Accepted 00th January 2014

DOI: 10.1039/x0xx00000x

www.rsc.org/

Hyungmin Park, Sinho Choi, Sungjun Lee, Gaeun Hwang, Nam-Soon Choi* and Soojin Park*

Despite Si being one of the most promising anode materials in lithium-ion batteries, significant challenges remain, including a large volume change, low electrical conductivity and high temperature operation for practical use. Herein, we demonstrate a facile synthesis of Si particles with double-shell coating layers, in which aluminum trifluoride (AlF₃) acts as an artificial defensive matrix, and carbon layers enhance electrical conductivity and compatibility with carbon black. Our study reveals that Si anodes with double shell layers composed of AlF₃ exhibit excellent electrochemical properties at 25 °C and 60 °C, owing to a formation of stable solid-electrolyte-interface layer on the Si surface, and good mechanical strength and chemical nature of AlF₃ layers. The Si@AlF₃@C anode shows a significantly improved cycling performance (capacity retention of 75.8% after 125 cycles at 25 °C and 73.7% at 60 °C after 150 cycles, compared to the specific capacity in the first cycle) and excellent rate capability of >1600mAh/g, even at a 5C rate (at 25 °C). Furthermore, the AlF₃ assisted Si electrode exhibits remarkably reduced volume expansion (thickness change of 71% after 125 cycle at 25 °C and 128% after 150 cycles at 60 °C).

Introduction

Since lithium-ion batteries (LIBs) have been commercialized in 1991, human life has changed a lot using electrical equipment operating from LIBs, like mobile phones, laptop computers, plug-in hybrid electric vehicles, hybrid electric vehicles, and full electric vehicles, due to the batteries' high energy storage and portable properties.¹ However, demand for energy is rapidly increased owing to a fast developing speed of advanced electronic devices. To meet the requirement of energy demand, it is essential to increase the energy, power density, and operation time of LIBs. Furthermore, LIBs should satisfy a stable operation at high temperature, to be use in vehicles, military equipment, and countries near the equator.²

Silicon (Si) is one of the most promising next generation anode materials in LIBs due to its high theoretical capacity (3579 mAh g⁻¹ for Li₁₅Si₄ at room temperature), low cost among Li hosting materials (e.g., Sn, Ge, CuO, SnO₂, etc.), and a low reaction potential of <0.4 V (versus Li/Li+).³ However, the large volume change during lithiation/delithiation processes leads to a pulverization of Si and a formation of thick insulating solid-electrolyte-interface (SEI) layers by the cracking of Si, resulting in significant capacity fading.^{4,7} That is why Si has not been used in commercialized LIBs.

These main challenges remain for practical usage of Si electrodes in LIBs. To overcome these problems, many types of Si structures have been suggested, such as Si thin film,⁸⁻¹¹ Si nanoparticles,¹²⁻¹⁵ Si nanotubes,¹⁶⁻¹⁸ Si nanowires,¹⁹⁻²² bulk porous Si²³⁻²⁷ and yolk-shell Si²⁸⁻³⁰, to enhance electrochemical performances at room temperature, including a high specific capacity and a stable cycling performance.

In addition, LIBs are increasingly required to stably operate at elevated temperatures of >60 °C, especially in a full electric vehicle application. Recent research of high temperature LIBs has focused on controlling non-liquid type electrolytes, such as gel polymers and solid state electrolytes. For example, poly(vinylidene fluoride-co-hexafluoropropylene),^{31, 32} polyacrylonitrile,³³⁻³⁶ poly(vinyl chloride)/poly(methyl methacrylate) blend,³⁷⁻³⁹ poly(ethylene oxide),⁴⁰⁻⁴³ and poly(styrene-*b*-ethylene oxide)⁴⁴ were investigated as polymer based electrolytes. Also, full solid state electrolytes were studied with Li₂S-P₂S₅,^{45, 46} Li₇La₃Zr₂O₁₂,⁴⁷⁻⁴⁹ Li₂O-V₂O₅-SiO₂,⁵⁰ and Li₂S-GeS₂-P₂S₅(thio-LISICON)⁵¹ for LIB operation at elevated temperatures, by reducing a serious side reaction at the interface between electrolyte and electrode. However, these electrolytes are still hindered for practical use due to several problems, including limited power by a low ionic

conductivity,^{49, 52-54} difficulty of high temperature synthesis in the case of solid state electrolyte,⁴⁹ and high cost. Meanwhile, conventional carbonate-based liquids and aqueous electrolytes showed unstable characteristics at elevated temperatures, including the formation of thick SEI layers and gas evolution (e.g., CO₂ and PF₅), due to a serious side reaction and the decomposition of electrolyte and lithium salt at the interface between Si electrode and electrolyte.⁵⁵⁻⁶⁰ In addition, volume expansion of Si electrodes could be maximized at elevated temperature.^{61, 62} In cases of manganese-based cathode materials, numerous studies have been explored with coating,⁶³⁻⁶⁵ structure alteration,⁶⁶ controlling electrolytes,⁶⁷ and additives^{68, 69} to resolve poor cycling properties due to Jahn-Teller distortion⁷⁰ at elevated temperatures.

Compared to electrolytes and cathode materials, the electrochemical properties of Si-based anode materials at elevated temperatures are rarely reported. Recently, Etacheri et al. reported that the distinctive surface chemistry of a Si nanowire electrode in 1,3-dioxolane-based electrolytes could remarkably improve the electrochemical properties of the Si electrode, including reduced irreversible capacity loss, stable reversible capacities over prolonged cycling at 60 °C, and lower impedance, compared to alkyl carbonate electrolytes.⁷¹ Other strategies include the introduction of artificial coating layers such as Cu,⁷² Ag,^{14, 73} Au,⁷⁴ NiO,⁷⁵ Ti_xSi_y,¹⁵ Al₂O₃,⁷⁶ conducting polymers,⁷⁷ TiN,⁷⁸ and carbon^{23, 79, 80} on the Si surfaces. These results showed reduced polarization and stabilized SEI layers formed on the surface of Si electrodes in conventional liquid electrolytes. Among them, Ti_xSi_y-coated Si electrodes showed excellent electrochemical performances in terms of cycling stability, rate capability, and remarkably reduced exothermic heat.¹⁵ Carbon-coated porous Si electrodes displayed considerable performance, assisted with a fluoroethylene carbonate (FEC) based electrolyte at elevated temperatures, due to a suppression of electrolyte decomposition.²³

Herein, we demonstrate a novel design of Si-based anode material exhibiting excellent electrochemical performances at 25 °C and 60 °C, in which double coating layers consisting of AlF₃ and amorphous carbon are introduced on a Si surface. The AlF₃ acts as an artificial defensive matrix for enhancing the mechanical strength and electrochemical stability of Si electrodes at 60 °C, while the outermost carbon layers play an important role in increasing the electrical conductivity of AlF₃-coated Si particles. Our investigations verify that AlF₃ layers provide strong enough mechanical strength to endure the volume expansion of Si electrodes during repeated long-term cycling at 25 °C and 60 °C. Compared to carbon-coated Si electrodes, Si electrodes coated with double layers exhibit a significantly improved cycling performance and reduced electrode thickness at 25 °C and 60 °C.

Experimental

Synthesis of AlF₃-coated Si nanoparticles: 1 g of Si nanoparticles (Alfa Aesar, an average diameter of 100 nm) were dispersed into 10 mL of 1 wt% hydrofluoric acid (HF, J.T. Baker) aqueous solution at room temperature in order to remove the native oxide layer, followed by rinsing with deionized (DI) water several times. Then, the obtained powder was completely dried in a vacuum oven at 80 °C for 24 h. HF-treated Si nanoparticles were dispersed in 25 mL of ethanol (J.T. Baker). A mixture of 0.1 mL [3-(2-Aminoethylamino)propyl] trimethoxysilane (AEAPTMS, Sigma Aldrich) and 25 mL DI water was added to the Si dispersed solution and stirred for 10 min at room temperature. After the reaction, the solution was filtered and dried in a vacuum oven at 80 °C for 12 h. To prepare AlF₃-coated Si nanoparticles, 0.1 M of aluminum nitrate nonahydrate (Sigma Aldrich) aqueous solution (10 mL for 7wt% AlF₃ relative to Si and 2.17 mL for 1.5 wt%) was mixed together with 1g of AEAPTMS coated Si nanoparticles. Subsequently, 0.6 M of ammonium fluoride (NH₄F, Sigma Aldrich) aqueous solution (5 mL for 7 wt% and 1.08 mL for 1.5 wt%) was added to the as-prepared solution. All mixtures were continuously stirred at 80 °C for 3 h and dried in a vacuum oven at 80 °C for 12 h to make AlF₃-coated Si particles.

Synthesis of Si@C and Si@AlF₃@C nanoparticles: To introduce carbon layers (carbon contents of ~10 wt%) onto the surface of Si and Si@AlF₃ nanoparticles, a chemical vapor deposition process of toluene (Sigma Aldrich) was performed in a quartz furnace (MTI, GSL-1100X) at 900 °C for 7 min.

Characterization of Si@C and Si@AlF₃@C particles: Transmission electron microscopy (TEM, JEM-1400) was used to investigate the morphologies of the Si@C and Si@AlF₃@C particles before and after cycles. Also, scanning electron microscopy (Nano SEM 230, FEI) was used to characterize the thickness change of Si electrodes before and after cycles at an accelerating voltage of 10 kV. X-ray diffractometer (D8 ADVANCE, Bruker) was employed to investigate the microstructures of Si, AlF₃ and carbon. A carbon coating layer on the Si surface was characterized by Raman spectrometer (Alpha 300s, WITec GmbH) operating with a laser excitation wavelength of 532 nm. X-ray photoelectron spectroscopy (K-alpha, Thermo Fisher) measurement was used to characterize the SEI layer formed on the surface of the Si@C and Si@AlF₃@C. An electrochemical impedance analysis was performed on the IVIUM frequency response analyzer ranging from 0.01 Hz to 100 KHz.

Electrochemical tests: The coin type half-cell (CR2016) was assembled to test the electrochemical properties of the Si@C and the Si@AlF₃@C electrodes. The Si electrodes were prepared by spreading a slurry mixture of surface modified Si powder as an active material, super P carbon black as conductive materials, and poly (acrylic acid) (PAA, weight average molecular weight = 100 kg/mol, Sigma Aldrich)/sodium carboxymethyl cellulose (CMC, 4wt% in H₂O, Sigma Aldrich) (PAA/CMC = 50/50, wt/wt) as polymeric binder with a weight ratio of 80:10:10 on a Cu foil. The electrochemical test was performed in the potential window from 0.005 to 2.0 V

(versus Li/Li⁺) with a battery measurement system (WonATech, WBCS 3000) at 25 °C and 60 °C. The electrolyte used was 1.3 M LiPF₆ in a mixture of ethylene carbonate (EC) and diethyl carbonate (DEC) (EC:DEC = 30:70, v/v) and 10% fluorinated ethylene carbonate (FEC) as an additive. Microporous polyethylene film (Celgard 2400) was used as a separator. Battery cell assembly and disassembly were carried out in argon-filled glove box with less than 1 ppm of both oxygen and moisture. After cycling, the cells were opened, rinsed with DMC for 1 h to remove residual Li salts and carbonate based electrolytes, and dried at room temperature in a glove box.

Results and discussion

Synthesis of AlF₃-coated Si particles

The surface modification process of Si particles with AlF₃ and amorphous carbon (Si@AlF₃@C) is schematically illustrated, as shown in Figure 1a. Before applying the AlF₃ coating to a Si surface, the native oxide layer on the surface of Si particles was removed by hydrofluoric acid (HF). TEM image shows that the silicon oxide layers were mostly removed from the Si particle (Fig. 1b). Subsequently, the AlF₃ coating layers were introduced on the surface of HF-treated Si nanoparticles. Firstly, 0.1 mL of [3-(2-aminoethylamino)propyl] trimethoxysilane (AEAPTMS) was dissolved in 25 mL of deionized water and 1 g of Si nanoparticles was added with vigorous stirring for 10 min at room temperature to make AEAPTMS-modified Si particles. Secondly, 0.1 M of aqueous aluminum nitrate solution, 1g of dried AEAPTMS modified Si, and 0.6 M of aqueous ammonium fluoride solution were mixed together and stirred at 80 °C for 3 hr to synthesize AlF₃-coated Si (Si@AlF₃) nanoparticles. When 2 mL of 0.1 M aluminum precursors were used, AlF₃ layers of 5-6 nm were uniformly coated on the surface of the Si particles (Fig. 1c). With an increasing concentration of 0.1 M aluminum precursor (10 mL), thick AlF₃ layers of 15-20 nm could be introduced onto the Si surface (Fig. 1d). To confirm the existence of the AlF₃ layers, X-ray diffraction (XRD) patterns were obtained from the Si particles with 5-6 nm thick AlF₃ layers (Fig. 1e). All XRD peaks correspond to pure crystalline Si. Also, AlF₃ is not detected, even though 1.5 wt% of AlF₃ was confirmed by an energy dispersive X-ray spectroscopy (EDS) analysis (see ESI, Fig. S1). Presumably, the amount of AlF₃ was not enough to detect with XRD, due to the detection limit or the amorphous AlF₃ layers were coated on the Si surface. In contrast, when 7wt% of AlF₃ was coated on the Si particles, XRD peaks corresponding to crystalline AlF₃ were clearly seen (Fig. 1f). It suggested that a thin AlF₃ layer (5-6 nm thick) was successfully coated on the Si surface (Fig. 1c), but the XRD peaks of the AlF₃ were not detected owing to the detection limit. In addition, we confirmed the uniform coating of the AlF₃ by using selective etching of Si nanoparticles. When the AlF₃-coated Si particles (seen in Fig. 1d) were immersed in 5% of sodium hydroxide (NaOH), the inner crystalline Si was completely dissolved and AlF₃ hollow structures were observed without

changing the AlF₃ thickness, compared to pristine AlF₃-coated Si (Fig. 1g). Furthermore, the EDS measurement of AlF₃-coated Si particles showed the uniform coating of the AlF₃ on the surface of Si nanoparticles (ESI, Fig. S1).

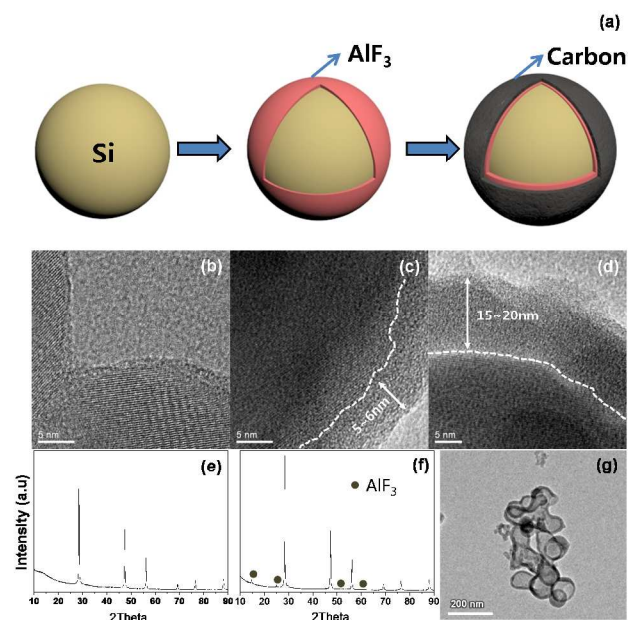


Fig. 1 (a) schematic illustration showing synthetic process of Si@AlF₃@C particle. TEM images of (b) HF-treated Si nanoparticles, (c) Si particles with thin AlF₃ coating layer, and (d) Si particles with thick AlF₃ layers. XRD patterns of Si particles with (e) thin and (f) thick AlF₃ coating layers. (g) AlF₃ hollow structure obtained by NaOH etching of Si from sample seen in Figure 1d.

As seen in Figure 1, AlF₃ was successfully introduced on the Si surface, and a high mechanical property of the AlF₃ would be helpful in Si-based anode material for LIBs. However, the poor electrical conductivity of the AlF₃-coated Si can be a serious problem for high-power Si-based batteries. To increase the electrical conductivity of the AlF₃-coated Si (5-6 nm thick AlF₃) nanoparticles, amorphous carbon layers were introduced using a chemical vapor deposition (CVD) process of toluene at 900 °C for 7 min.⁸¹ The carbon contents of 10 wt% were confirmed by elemental analysis. The TEM image of the carbon-coated Si (Si@C) nanoparticle shows that 5-7 nm thick carbon layers were uniformly coated on the Si surface (Fig. 2a). When the same carbon coating process was applied to AlF₃-coated Si particles, 5-8 nm thick carbon layers were coated on the surface of the AlF₃ layers (Fig. 2b). Carbon prepared from the CVD process of toluene vapor was characterized by Raman spectroscopy. The Raman spectrum obtained from carbon-coated Si particles shows that the ratio of the disordered (D) band and graphene (G) band (D/G ratio) is 1.84, indicating the characteristics of amorphous carbon (Fig. 2c). After carbon coating, the XRD patterns of AlF₃-coated Si particles are a quite similar to those of the pristine AlF₃-coated Si sample,

suggesting that carbon coating does not affect the microstructure of the AlF_3 and Si (Fig. 2d).

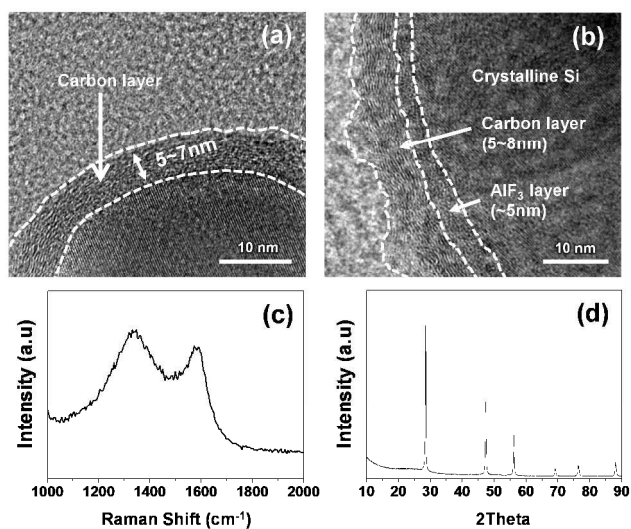


Fig. 2 TEM images of (a) Si@C nanoparticles and (b) $\text{Si@AlF}_3\text{@C}$ nanoparticles. (c) Raman spectrum of Si@C nanoparticles and (d) XRD pattern of $\text{Si@AlF}_3\text{@C}$ nanoparticles show that amorphous carbon layers are coated on the surface of Si and Si@AlF_3 particles.

Electrochemical performances of AlF_3 -coated Si anode

We investigated the electrochemical properties of two Si-based anode materials (Si@C and $\text{Si@AlF}_3\text{@C}$) assembled with a coin type half-cell in a range of 0.005–2.0 V (versus Li/Li^+). Figure 3a shows the first cycle voltage profiles of Si@C and $\text{Si@AlF}_3\text{@C}$ electrodes obtained at a rate of C/20. The Si@C electrode shows a high initial coulombic efficiency (ICE) of 86.9% with a discharging (lithiation) capacity of 2808 mAh g^{-1} and a charging (delithiation) capacity of 2441 mAh g^{-1} . In contrast, the $\text{Si@AlF}_3\text{@C}$ electrode exhibits an initial coulombic efficiency of 81.8% with a discharging capacity of 2457 mAh g^{-1} at the same rate. It may be attributed to the reduced electrical conductivity by the insulating AlF_3 layers at the interface between Si and carbon, compared to Si@C system. However, the $\text{Si@AlF}_3\text{@C}$ electrode shows much more stable cycling performance at a rate of C/2 with a specific charge capacity of 1001 mAh g^{-1} after 125 cycles at 25°C , corresponding to the capacity retention of 75.8%. In contrast, the Si@C electrode exhibits a poor cycling retention of 501 mAh g^{-1} after 125 cycles at a same rate. It may be attributed to a formation of a thick SEI layer in the Si@C electrodes, as will be discussed later. This result suggests that only carbon coating is not enough to achieve a highly stable cycling property of Si-based anode materials. In the case of the $\text{Si@AlF}_3\text{@C}$ electrode, since the AlF_3 layers act as an artificial defensive matrix which may form a stable SEI layer and accommodate a large volume change of a Si electrode due to its good mechanical property, highly stable cycling performance was obtained.

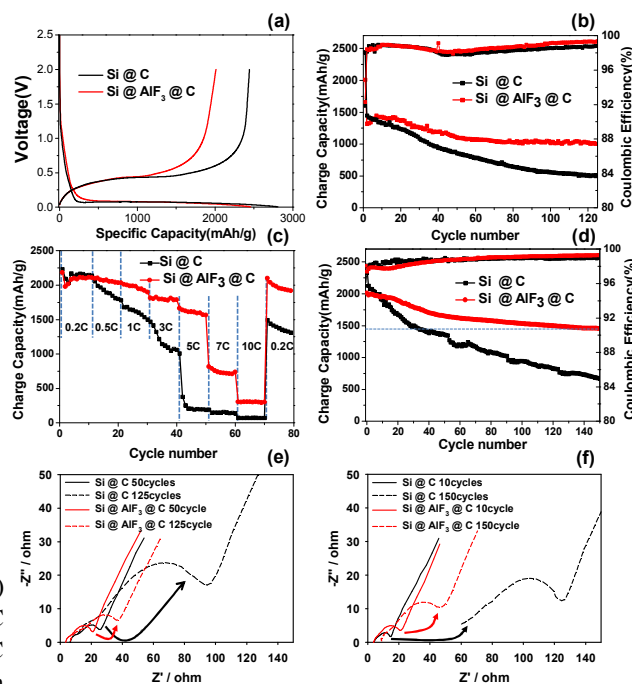


Fig. 3 Electrochemical performances of Si@C and $\text{Si@AlF}_3\text{@C}$ electrodes. (a) First cycle discharge and charge curves of Si@C and $\text{Si@AlF}_3\text{@C}$ electrodes obtained in the range of 0.005–2.0 V at a rate of C/20. (b) Cycling performances and (c) rate capabilities of Si@C and $\text{Si@AlF}_3\text{@C}$ electrodes obtained with a rate of C/2 at 25°C . (d) Cycling performances of Si@C and $\text{Si@AlF}_3\text{@C}$ electrodes obtained with a rate of C/2 at 60°C . Impedance spectra of Si@C and $\text{Si@AlF}_3\text{@C}$ electrodes obtained at (e) 25°C and (f) 60°C .

Moreover, we investigated the rate capabilities of Si@C and $\text{Si@AlF}_3\text{@C}$ electrodes at various C-rates (Fig. 3c). The charge capacity of the Si@C electrode was dramatically decreased at variable discharge rates with a fixed lithiation of C/5. In contrast, the $\text{Si@AlF}_3\text{@C}$ electrode exhibited remarkably enhanced rate capabilities (1600 mAh g^{-1} even at a 5C rate) in the same test. After 70 cycles, the charge capacity of $\text{Si@AlF}_3\text{@C}$ was mostly recovered to the original specific capacity. This result suggests that both the electrical conductivity and structural integrity of Si-based electrodes during repeated cycling play a key role in enhancing rate capabilities.

For practical LIB applications, an electrochemical test at elevated temperatures is required. We investigated the electrochemical performances of both Si@C and $\text{Si@AlF}_3\text{@C}$ electrodes at 60°C in a coin-type half-cell. Since the operation temperature increases, the diffusion of lithium ion is faster, resulting in an increase of specific capacity. The Si@C electrode showed a high specific capacity of 2126 mAh g^{-1} in the first cycle, and 674 mAh g^{-1} after 150 cycles at a rate of

C/2. The poor cycling stability may be attributed to a formation of thick SEI layers on the Si@C surface due to a severe decomposition of the electrolyte at 60 °C.

On the contrary, the Si@AlF₃@C electrode exhibited highly stable cycle performance with a specific capacity of 1977 mAh g⁻¹ in the first cycle and 1457 mAh g⁻¹ after 150 cycles at a rate of C/2, corresponding to the capacity retention of 73.7%. To further understand the superior electrochemical properties of the Si@AlF₃@C electrode, an electrochemical impedance spectroscopy (EIS) measurement was employed. Si@AlF₃@C electrode showed slightly larger impedance value than that of Si@C electrode due to AlF₃ insulating property (see ESI, Fig. S2). However, both the Si@C and Si@AlF₃@C electrodes exhibited similar ohmic and charge transfer resistance until 50 cycles at 25 °C (Fig. 3e). After 125 cycles, the Si@C electrode showed a tremendously increased charge transfer resistance (3 times larger than that of the electrode after 50 cycles). In contrast, the Si@AlF₃@C electrode displayed much less increased resistance after 125 cycles. The difference of resistance between the Si@C and the Si@AlF₃@C electrodes was significantly increased at the elevated temperature of 60 °C. In the case of the Si@AlF₃@C electrode, the 150-cycled electrode exhibited a slightly increased resistance value at 60 °C, compared to the 125-cycled electrode at 25 °C. However, the Si@C electrode showed tremendously increased resistance, owing to the formation of thick SEI layers by a serious decomposition of the electrolyte at 60 °C.

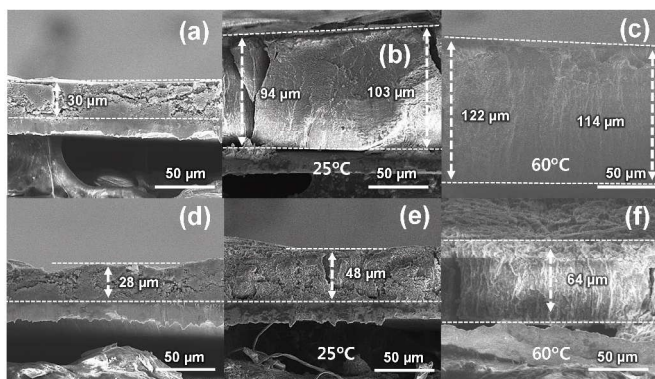


Fig. 4 Cross-sectional SEM images of Si@C and Si@AlF₃@C electrodes showing volume expansion after cycling. SEM images of Si@C electrodes (a) before, (b) after 125 cycles at 25 °C, and (c) after 150 cycles at 60 °C. SEM images of Si@AlF₃@C electrodes (d) before, (e) after 125 cycles at 25 °C, and (f) after 150 cycles at 60 °C.

In addition to stable cycling retention, swelling of electrodes after cycling is also a critical issue in battery anodes. We obtained cross-sectional SEM images from pristine and cycled electrodes (125 cycle at 25 °C and 150 cycles at 60 °C), as shown in Figure 4. The 30 μm thick pristine Si@C electrode showed a tremendous thickness alternation (94-103 μm corresponding to 213-243% expansion) after 125 cycle at 25 °C (Fig. 4b). At an elevated temperature of 60 °C, the thickness of the electrodes was further increased to expansion of 280-306%

(Fig. 4c). In particular, when the 150-cycled Si@C electrode was disassembled in an argon-filled glove box, most electrolytes were dried, indicating that a serious decomposition of the electrolytes had occurred. Compared to the Si@C electrodes, the Si@AlF₃@C electrode showed a much lower volume expansion of 71% and 128% at 25 °C and at 60 °C, respectively (Fig. 4d-4f). These results suggest that the AlF₃ layer between the Si and carbon can restrict a large volume change of the Si electrodes and form a stable SEI layer, compared to the Si@C electrode.

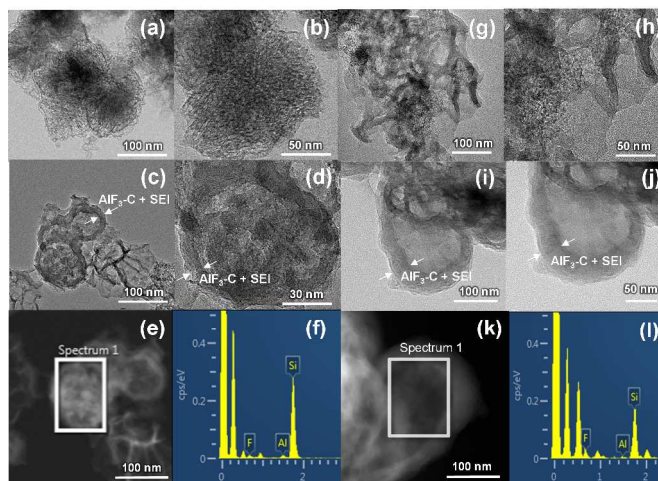


Fig. 5 TEM images of Si@C and Si@AlF₃@C particles after 125 cycles at 25 °C and 150 cycles at 60 °C. TEM images of Si@C ((a) low- and (b) high-magnification obtained at 25 °C; (g) low- and (h) high-magnification obtained at 60 °C) and Si@AlF₃@C ((c) low- and (d) high-magnification obtained at 25 °C; (i) low- and (j) high-magnification obtained at 60 °C). HAADF images of Si@AlF₃@C particles obtained after cycling at (e) 25 °C and (f) 60 °C, and the EDS results obtained from selected area ((f) sample seen in Fig. 5e and (l) sample seen in fig. 5k) showing existence of Al and F elements.

As further evidence for stable cycling of the Si@AlF₃@C electrode, we obtained TEM images of Si particles after 125 cycles at 25 °C and after 150 cycles at 60 °C. Figure 5a shows a low-magnified TEM image of expanded Si@C particles after 125 cycles. In the magnified image, sponge-like Si@C structures were observed as being similar to those Iwamura et al. reported previously (Fig. 5b).^[80] In contrast, the Si@AlF₃@C particles maintained the original dimensions, except for the trapping of amorphous Si particles within the AlF₃@C hollow structure at 25 °C (Fig. 5c). In the magnified TEM image of Figure 5d, the shell thickness of a hollow structure consisting of AlF₃, carbon and SEI layers are 13-18 nm, which is slightly increased compared to the thickness of AlF₃@C in the original Si@AlF₃@C particles. It may be attributed to the sufficient mechanical strength of the AlF₃ protective layers. To prove the elements of Si, Al and F, the high-angle annular dark field (HAADF) TEM image of the sample seen in Figure 5c was obtained (Fig. 5e), and the EDS analysis (from the rectangular area seen in Fig. 1e) was

performed (Fig. 5f). From these results, the AlF_3 and carbon layers in the $\text{Si}@/\text{AlF}_3/\text{C}$ particles were still strongly adhered to the amorphous Si after 125 cycles at 25 °C. At the elevated temperature of 60 °C, the morphology of $\text{Si}@/\text{C}$ particles after 150 cycles seems to be a significantly expanded sponge-like structure, due to a serious side reaction at the higher temperature (Fig. 5g and 5h). The TEM image of $\text{Si}@/\text{AlF}_3/\text{C}$ particles also showed a volume expansion of particles, but a hollow shell consisting of AlF_3 , carbon, and SEI layers still remained after cycling (Fig. 5i and 5j). The HAADF TEM image and EDS analyses of the sample seen in Figure 5i indicated that cycled Si particles are composed of Si, AlF_3 and carbon. Even after long-term cycling at 60 °C, the double coating layers of AlF_3 and carbon play an important role in keeping the mechanical integrity of the Si-based particles.

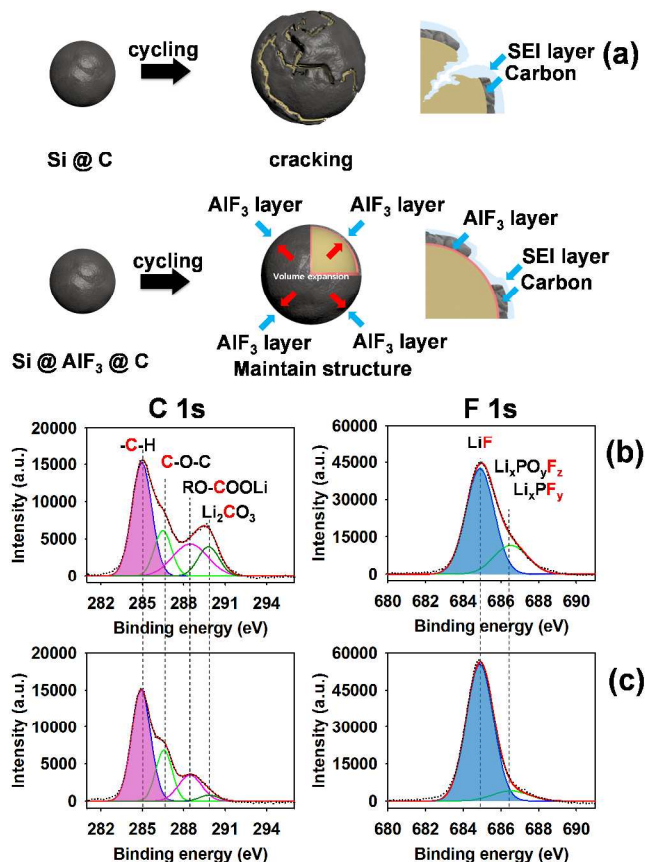


Fig. 6 (a) Schematic illustration showing cracking mechanism of Si particles with and without AlF_3 layers. XPS spectra with C 1s and F 1s of (b) $\text{Si}@/\text{C}$ and (c) $\text{Si}@/\text{AlF}_3/\text{C}$ electrodes after 150 cycles at 60 °C.

Proposed mechanism of SEI layer formation

Figure 6a displays possible mechanisms for the cracking of Si anode materials with and without AlF_3 . The interfacial layers with only amorphous carbon can readily break due to a weak mechanical strength of carbon anchored on the Si particles, and thus thick SEI layers are produced via continuous unwanted electrolyte decomposition on the exposed active Si surface.

Importantly, a mechanically stable AlF_3 layer uniformly covering the Si surface could effectively endure a large volume change of Si particles during cycling, while the outer amorphous carbon shell is partially disconnected, as depicted in Fig. 6a. In this regard, the AlF_3 layer coated on the Si particle is expected to avoid the direct contact of the electrolyte with the Si active materials and alleviate the undesirable electrolyte decomposition. Also, the chemical nature of AlF_3 can promote formation of stable SEI layers due to its unreactive characteristics with electrolyte and HF species.⁸² The effect of AlF_3 coating layer on the interaction between Si electrode surface and electrolyte was characterized by XPS analyses. To investigate the surface chemistry of both $\text{Si}@/\text{C}$ and $\text{Si}@/\text{AlF}_3/\text{C}$ electrodes after 150 cycles at 60 °C, XPS measurements of cycled Si anodes were performed, as shown in Fig. 6b. In C 1s spectra, the pronounced peak corresponding to carbon bonded to hydrogen (C-H) was observed at 285.0 eV for both electrodes with similar levels of intensity. A noticeable feature in the C 1s XPS spectra of Fig. 6b is that the $\text{Si}@/\text{AlF}_3/\text{C}$ electrode exhibits a significantly reduced peak intensity attributed to Li_2CO_3 , which is generated by the EC decomposition,⁸³ compared to the $\text{Si}@/\text{C}$ electrode. This result suggests that interfacial architecture based on the AlF_3 coating layer inhibits the reductive decomposition of the EC solvent at the Si anode. The LiF peak at 684.9 eV appeared for both electrodes. This is because using FEC as a reducible additive produces an SEI layer mainly composed of LiF.⁸⁴ The C1s XPS spectrum obtained from the $\text{Si}@/\text{C}$ electrode showed a relatively strong peak ascribed to $\text{Li}_x\text{PO}_y\text{F}_z$ and Li_xPF_y at 687 eV, compared with the $\text{Si}@/\text{AlF}_3/\text{C}$ electrode. This is persuasive evidence that the AlF_3 coating layer effectively suppresses LiPF_6 salt decomposition.

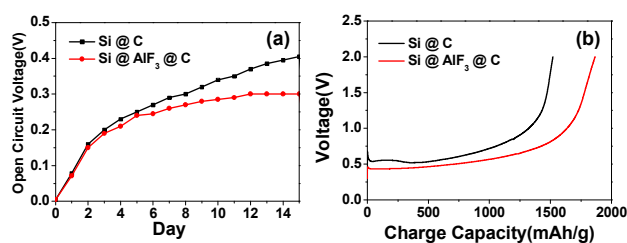


Fig. 7 (a) Open circuit voltage plots of fully lithiated $\text{Si}@/\text{C}$ and $\text{Si}@/\text{AlF}_3/\text{C}$ electrodes obtained at 60 °C. (b) Lithium extraction voltage profiles of $\text{Si}@/\text{C}$ and $\text{Si}@/\text{AlF}_3/\text{C}$ electrodes after 15 days at 60 °C (samples seen in Figure 7a).

The open circuit voltage (OCV) variation of fully lithiated $\text{Si}@/\text{C}$ and $\text{Si}@/\text{AlF}_3/\text{C}$ electrodes stored at 60 °C was monitored, as shown in Fig. 7a. The OCV of the fully lithiated $\text{Si}@/\text{C}$ electrode continuously increased for 15 days, whereas the fully lithiated $\text{Si}@/\text{AlF}_3/\text{C}$ electrode showed a lower OCV increase. This indicates that the AlF_3 coating layer effectively restrains the self-discharging behavior by preventing some side reactions between the Si electrode and the electrolyte. Figure 7b presents the voltage profiles of lithiated $\text{Si}@/\text{C}$ and $\text{Si}@/\text{AlF}_3/\text{C}$ electrodes during the Li extraction after they were

stored at 60 °C for 15 days (seen in Fig. 7a). The charge capacity of the Si@C electrode significantly declined to 1520 mAh g⁻¹ (a value of approximately 63 % relative to the Si@C electrode before storing) after storage. On the other hand, the Si@AlF₃@C electrode maintained a superior specific capacity of 1865 mAh g⁻¹ (a value of approximately 92.7% relative to the Si@AlF₃@C electrode before storing) under the same condition. This implies that the AlF₃ coating layer is very effective to prevent the Li extraction from the Si electrode indicating the self-discharge.

Conclusion

We demonstrated a facile synthesis of Si nanoparticles with double shell layers, in which AlF₃ layers enhance the mechanical and electrochemical stability while amorphous carbon increases the electrical conductivity of Si particles. Synergistic coupling of AlF₃ and amorphous carbon layers enabled the Si anode to exhibit significantly improved long-term cycling stability at 25 °C, and even at a high temperature of 60 °C. Moreover, the AlF₃ assisted Si electrode showed remarkably reduced volume expansion (a thickness change of 71% after 125cycle at 25 °C and 128% after 150 cycles at 60 °C). This novel design of a Si anode with double shell layers can be extended to other lithium alloying materials (e.g., germanium and tin) which have a large volume change during the lithiation and delithiation process.

Acknowledgements

This work was supported by the IT R&D program of MOTIE/KEIT (10046309).

Notes and references

Interdisciplinary School of Green Energy, Ulsan National Institute of Science and Technology, Ulsan 689-798, Republic of Korea. Fax: +82-52-217-2909; Tel: +82-52-217-2515

E-mail: nschoi@unist.ac.kr and spark@unist.ac.kr

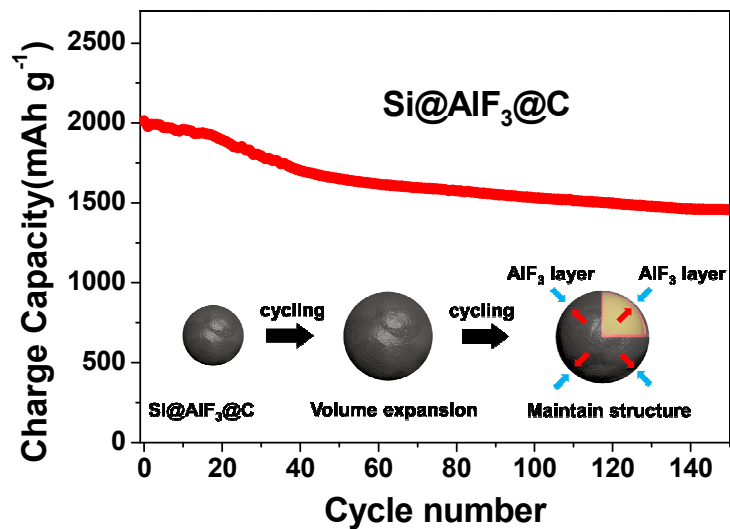
† Electronic Supplementary Information (ESI) available: EDS measurement of Si@AlF₃@C particles and EIS measurement of both Si@C and Si@AlF₃@C electrodes. See DOI:10.1002/xxxx

- 1 Y. Wang, J. Yi and Y. Xia, *Adv. Energy. Mater.*, 2012, **2**, 830-840.
- 2 J. M. Tarascon and M. Armand, *Nature*, 2001, **414**, 359-367.
- 3 V. Etacheri, R. Marom, R. Elazari, G. Salitra and D. Aurbach, *Energy Environ. Sci.*, 2011, **4**, 3243-3262.
- 4 U. Kasavajjula, C. Wang and A. J. Appleby, *J. Power Sources*, 2007, **163**, 1003-1039.
- 5 A. Magasinski, P. Dixon, B. Hertzberg, A. Kvit, J. Ayala and G. Yushin, *Nat. Mater.*, 2010, **9**, 353-358.
- 6 J. R. Szczech and S. Jin, *Energy Environ. Sci.*, 2011, **4**, 56-72.
- 7 H. Wu and Y. Cui, *Nano Today*, 2012, **7**, 414-429.
- 8 J. P. Maranchi, A. F. Hepp and P. N. Kumta, *Electrochem. Solid-State Lett.*, 2003, **6**, A198-A201.
- 9 V. Baranchugov, E. Markevich, E. Pollak, G. Salitra and D. Aurbach, *Electrochem. Commun.*, 2007, **9**, 796-800.
- 10 J. P. Maranchi, A. F. Hepp, A. G. Evans, N. T. Nuhfer and P. N. Kumta, *J. Electrochem. Soc.*, 2006, **153**, A1246-A1253.
- 11 J. Yin, M. Wada, K. Yamamoto, Y. Kitano, S. Tanase and T. Sakai, *J. Electrochem. Soc.*, 2006, **153**, A472-A477.
- 12 T. H. Hwang, Y. M. Lee, B.-S. Kong, J.-S. Seo and J. W. Choi, *Nano Lett.*, 2011, **12**, 802-807.

- 13 S. Xun, X. Song, L. Wang, M. E. Grass, Z. Liu, V. S. Battaglia and G. Liu, *J. Electrochem. Soc.*, 2011, **158**, A1260-A1266.
- 14 S. Yoo, J.-I. Lee, S. Ko and S. Park, *Nano Energy*, 2013, **2**, 1271-1278.
- 15 O. Park, J.-I. Lee, M.-J. Chun, J.-T. Yeon, S. Yoo, S. Choi, N.-S. Choi and S. Park, *RSC Adv.*, 2013, **3**, 2538-2542.
- 16 M.-H. Park, M. G. Kim, J. Joo, K. Kim, J. Kim, S. Ahn, Y. Cui and J. Cho, *Nano Lett.*, 2009, **9**, 3844-3847.
- 17 T. Song, J. Xia, J.-H. Lee, D. H. Lee, M.-S. Kwon, J.-M. Choi, J. Wu, S. K. Doo, H. Chang, W. I. Park, D. S. Zang, H. Kim, Y. Huang, K.-C. Hwang, J. A. Rogers and U. Paik, *Nano Lett.*, 2010, **10**, 1710-1716.
- 18 Z. Wen, G. Lu, S. Mao, H. Kim, S. Cui, K. Yu, X. Huang, P. T. Hurley, O. Mao and J. Chen, *Electrochem. Commun.*, 2013, **29**, 67-70.
- 19 C. K. Chan, R. N. Patel, M. J. O'Connell, B. A. Korgel and Y. Cui, *ACS Nano*, 2010, **4**, 1443-1450.
- 20 K. Peng, J. Jie, W. Zhang and S.-T. Lee, *Appl. Phys. Lett.*, 2008, **93**, -.
- 21 C. K. Chan, R. Ruffo, S. S. Hong and Y. Cui, *J. Power Sources*, 2009, **189**, 1132-1140.
- 22 M. Ge, J. Rong, X. Fang and C. Zhou, *Nano Lett.*, 2012, **12**, 2318-2323.
- 23 M.-J. Chun, H. Park, S. Park and N.-S. Choi, *RSC Adv.*, 2013, **3**, 21320-21325.
- 24 H. Kim, B. Han, J. Choo and J. Cho, *Angew. Chem. Int. Ed.*, 2008, **47**, 10151-10154.
- 25 B. M. Bang, J.-I. Lee, H. Kim, J. Cho and S. Park, *Adv. Energy. Mater.*, 2012, **2**, 878-883.
- 26 J. Cho, *J. Mater. Chem.*, 2010, **20**, 4009-4014.
- 27 R. Yi, F. Dai, M. L. Gordin, H. Sohn and D. Wang, *Adv. Energy. Mater.*, 2013, **3**, 1507-1515.
- 28 N. Liu, H. Wu, M. T. McDowell, Y. Yao, C. Wang and Y. Cui, *Nano Lett.*, 2012, **12**, 3315-3321.
- 29 L. Pan, H. Wang, D. Gao, S. Chen, L. Tan and L. Li, *Chem. Commun.*, 2014, **50**, 5878-5880.
- 30 Z. Sun, X. Song, P. Zhang and L. Gao, *RSC Adv.*, 2014, **4**, 20814-20820.
- 31 L. Zhou, Q. Cao, B. Jing, X. Wang, X. Tang and N. Wu, *J. Power Sources*, 2014, **263**, 118-124.
- 32 C.-C. Yang, Z.-Y. Lian, S. J. Lin, J.-Y. Shih and W.-H. Chen, *Electrochim. Acta.*, 2014, **134**, 258-265.
- 33 B. Kurc, *Electrochim. Acta.*, 2014, **125**, 415-420.
- 34 P.-L. Kuo, C.-A. Wu, C.-Y. Lu, C.-H. Tsao, C.-H. Hsu and S.-S. Hou, *ACS Appl. Mater. Interfaces*, 2014, **6**, 3156-3162.
- 35 P. Carol, P. Ramakrishnan, B. John and G. Cheruvally, *J. Power Sources*, 2011, **196**, 10156-10162.
- 36 H.-R. Jung, D.-H. Ju, W.-J. Lee, X. Zhang and R. Kotek, *Electrochim. Acta.*, 2009, **54**, 3630-3637.
- 37 N.-S. Choi and J.-K. Park, *Electrochim. Acta.*, 2001, **46**, 1453-1459.
- 38 A. M. Stephan, T. P. Kumar, N. G. Renganathan, S. Pitchumani, R. Thirunakaran and N. Muniyandi, *J. Power Sources*, 2000, **89**, 80-87.
- 39 S. Rajendran and T. Uma, *Mater. Lett.*, 2000, **44**, 242-247.
- 40 F. Croce, G. B. Appetecchi, L. Persi and B. Scrosati, *Nature*, 1998, **394**, 456-458.
- 41 E. Quartarone, P. Mustarelli and A. Magistris, *Solid. State. Ionics.*, 1998, **110**, 1-14.
- 42 J. Xi and X. Tang, *Chem. Phys. Lett.*, 2004, **393**, 271-276.
- 43 Y.-T. Kim and E. S. Smotkin, *Solid. State. Ionics.*, 2002, **149**, 29-37.
- 44 E. D. Gomez, A. Panday, E. H. Feng, V. Chen, G. M. Stone, A. M. Minor, C. Kisielowski, K. H. Downing, O. Borodin, G. D. Smith and N. P. Balsara, *Nano Lett.*, 2009, **9**, 1212-1216.
- 45 F. Mizuno, S. Hama, A. Hayashi, K. Tadanaga, T. Minami and M. Tatsumisago, *Chem. Lett.*, 2002, **31**, 1244-1245.
- 46 M. Tatsumisago, S. Hama, A. Hayashi, H. Morimoto and T. Minami, *Solid. State. Ionics.*, 2002, **154-155**, 635-640.
- 47 H. Buschmann, J. Dolle, S. Berendts, A. Kuhn, P. Bottke, M. Wilkening, P. Heitjans, A. Senyshyn, H. Ehrenberg, A. Lotnyk, V. Duppel, L. Kienle and J. Janek, *Phys. Chem. Chem. Phys.*, 2011, **13**, 19378-19392.
- 48 J. Tan and A. Tiwari, *ECS Solid State Letters*, 2012, **1**, Q57-Q60.
- 49 R. Murugan, V. Thangadurai and W. Weppner, *Angew. Chem. Int. Ed.*, 2007, **46**, 7778-7781.
- 50 N. Kuwata, J. Kawamura, K. Toribami, T. Hattori and N. Sata, *Electrochem. Commun.*, 2004, **6**, 417-421.
- 51 R. Kanno and M. Murayama, *J. Electrochem. Soc.*, 2001, **148**, A742-A746.
- 52 M. Armand, F. Endres, D. R. MacFarlane, H. Ohno and B. Scrosati, *Nat. Mater.*, 2009, **8**, 621-629.

- 53 A. M. Christie, S. J. Lilley, E. Staunton, Y. G. Andreev and P. G. Bruce, *Nature*, 2005, **433**, 50-53.
- 54 W. H. Meyer, *Adv. Mater.*, 1998, **10**, 439-448.
- 55 M. Holzapfel, H. Buqa, L. J. Hardwick, M. Hahn, A. Würsig, W. Scheifele, P. Novák, R. Kötz, C. Veit and F.-M. Petrat, *Electrochim. Acta.*, 2006, **52**, 973-978.
- 56 M. Holzapfel, A. Würsig, W. Scheifele, J. Vetter and P. Novák, *J. Power Sources*, 2007, **174**, 1156-1160.
- 57 J. H. Ryu, J. W. Kim, Y.-E. Sung and S. M. Oh, *Electrochem. Solid-State Lett.*, 2004, **7**, A306-A309.
- 58 Y. Oumellal, N. Delpuech, D. Mazouzi, N. Dupre, J. Gaubicher, P. Moreau, P. Soudan, B. Lestriez and D. Guyomard, *J. Mater. Chem.*, 2011, **21**, 6201-6208.
- 59 Z. Zeng, W.-I. Liang, H.-G. Liao, H. L. Xin, Y.-H. Chu and H. Zheng, *Nano Lett.*, 2014, **14**, 1745-1750.
- 60 S. E. Sloop, J. B. Kerr and K. Kinoshita, *J. Power Sources*, 2003, **119-121**, 330-337.
- 61 R. A. Sharma and R. N. Seefurth, *J. Electrochem. Soc.*, 1976, **123**, 1763-1768.
- 62 B. A. Boukamp, G. C. Lesh and R. A. Huggins, *J. Electrochem. Soc.*, 1981, **128**, 725-729.
- 63 G. G. Amatucci, C. N. Schmutz, A. Blyr, C. Sigala, A. S. Gozdz, D. Larcher and J. M. Tarascon, *J. Power Sources*, 1997, **69**, 11-25.
- 64 J.-Z. Kong, C. Ren, G.-A. Tai, X. Zhang, A.-D. Li, D. Wu, H. Li and F. Zhou, *J. Power Sources*, 2014, **266**, 433-439.
- 65 W. H. Jang, M. C. Kim, S. N. Lee, J. Y. Ahn, V. Aravindan and Y. S. Lee, *J. Alloys Compd.*, 2014, **612**, 51-55.
- 66 Y. Xia and M. Yoshio, *J. Power Sources*, 1997, **66**, 129-133.
- 67 N.-S. Choi, J.-T. Yeon, Y.-W. Lee, J.-G. Han, K. T. Lee and S.-S. Kim, *Solid. State Ionics.*, 2012, **219**, 41-48.
- 68 T. Huang, M. Wu, W. Wang, Y. Pan and G. Fang, *J. Power Sources*, 2014, **262**, 303-309.
- 69 S.-Y. Ha, J.-G. Han, Y.-M. Song, M.-J. Chun, S.-I. Han, W.-C. Shin and N.-S. Choi, *Electrochim. Acta.*, 2013, **104**, 170-177.
- 70 M. S. Whittingham, *Chem. Rev.*, 2004, **104**, 4271-4302.
- 71 V. Etacheri, U. Geiger, Y. Gofer, G. A. Roberts, I. C. Stefan, R. Fasching and D. Aurbach, *Langmuir*, 2012, **28**, 6175-6184.
- 72 J.-P. Yen, C.-C. Chang, Y.-R. Lin, S.-T. Shen and J.-L. Hong, *J. Alloys Compd.*, 2014, **598**, 184-190.
- 73 Y. Yu, L. Gu, C. Zhu, S. Tsukimoto, P. A. van Aken and J. Maier, *Adv. Mater.*, 2010, **22**, 2247-2250.
- 74 M. Thakur, M. Isaacson, S. L. Sinsabaugh, M. S. Wong and S. L. Biswal, *J. Power Sources*, 2012, **205**, 426-432.
- 75 M. C. Qiu, L. W. Yang, X. Qi, J. Li and J. X. Zhong, *ACS Appl. Mater. Interfaces*, 2010, **2**, 3614-3618.
- 76 E. M. Lotfabad, P. Kalisvaart, A. Kohandehghan, K. Cui, M. Kupsta, B. Farbod and D. Mitlin, *J. Mater. Chem. A.*, 2014, **2**, 2504-2516.
- 77 Y. Yao, N. Liu, M. T. McDowell, M. Pasta and Y. Cui, *Energy Environ. Sci.*, 2012, **5**, 7927-7930.
- 78 D. Tang, R. Yi, M. L. Gordin, M. Melnyk, F. Dai, S. Chen, J. Song and D. Wang, *J. Mater. Chem. A.*, 2014, **2**, 10375-10378.
- 79 N. Dimov, S. Kugino and M. Yoshio, *Electrochim. Acta.*, 2003, **48**, 1579-1587.
- 80 M. Yoshio, H. Wang, K. Fukuda, T. Umeno, N. Dimov and Z. Ogumi, *J. Electrochem. Soc.*, 2002, **149**, A1598-A1603.
- 81 N. Dimov, K. Fukuda, T. Umeno, S. Kugino and M. Yoshio, *J. Power Sources*, 2003, **114**, 88-95.
- 82 Y.-K. Sun, M.-J. Lee, C. S. Yoon, J. Hassoun, K. Amine and B. Scrosati, *Adv. Mater.*, 2012, **24**, 1192-1196.
- 83 K. Xu, U. Lee, S. Zhang, M. Wood and T. R. Jow, *Electrochem. Solid-State Lett.*, 2003, **6**, A144-A148.
- 84 N.-S. Choi, K. H. Yew, K. Y. Lee, M. Sung, H. Kim and S.-S. Kim, *J. Power Sources*, 2006, **161**, 1254-1259.

Graphical Abstract



We demonstrate a facile method for synthesizing silicon particles with double coating layer consisting of aluminum trifluoride and amorphous carbon to use as anode material for high-performance lithium-ion battery at elevated temperature.
